Contributed paper

OPTO-ELECTRONICS REVIEW 9(1), 35–47 (2001)

# Strained layer SCH SQW InGaAs/GaAs lasers for 980-nm band

M. BUGAJSKI*[1] B. MROZIEWICZ[1], K. REGIŃSKI[1], J. MUSZALSKI[1], J. KUBICA[1], M. ZBROSZCZYK[1], P. SAJEWICZ[1], T. PIWOŃSKI[1], A. JACHYMEK[1], R. RUTKOWSKI[1], T. OCHALSKI[1], A. WÓJCIK[1], E. KOWALCZYK[1], A. MALĄG[2], A. KOZŁOWSKA[2], L. DOBRZAŃSKI[2], and A. JAGODA[2]

[1]Institute of Electron Technology, 32/46 Lotników Ave., 02-668 Warsaw, Poland
[2]Institute of Electronic Materials Technology, 133 Wólczyńska Str., 01-919 Warsaw, Poland

*Strained layer InGaAs/GaAs SCH SQW (separate confinement heterostructure single quantum well) lasers were grown by a molecular beam epitaxy (MBE). Highly reliable CW (continuous wave) 980-nm, broad contact, pump lasers were fabricated in stripe geometry using Schottky isolation and ridge waveguide construction. Threshold current densities of the order of* $J_{th} \approx 280$ *A/cm*$^2$ *(for the resonator length* $L = 700$ *μm) and differential efficiency* $\eta = 0.40$ *W/A (41%) from one mirror were obtained. The record wall-plug efficiency for AR/HR coated devices was equal to 54%. Theoretical estimations of above parameters, obtained by numerical modelling of devices were* $J_{th} = 210$ *A/cm*$^2$ *and* $\eta = 0.47$ *W/A from one mirror, respectively. Degradation studies revealed that uncoated and AR/HR coated devices did not show any appreciable degradation after 3000 hr of CW operation at 35°C heat sink temperature at the constant optical power (50 mW) conditions.*

**Keywords:** laser diodes, strained-layer semiconductor lasers.

## 1. Introduction

The development of erbium-doped fibre amplifiers (EDFAs) has enabled the proliferation of high-bandwidth data networks. $Er^{3+}$-doped fibre amplifiers coherently amplify 1550-nm signals through the conversion of 980-nm pump laser light [1]. Because the process is all optical, many signals can be amplified simultaneously with no delay and minimal electronics. The use of 980-nm pump wavelength has also another advantage as no excited state absorption exists for this wavelength. The pump lasers powering EDFAs must be highly reliable and at the same time have to provide maximum amplification power. All practical 980-nm lasers are based on the ternary AlGaAs and InGaAs alloys. The excellent lattice match, refractive index contrast, and thermal conductivity of AlGaAs give a freedom to optimise the vertical laser structure, while a single pseudomorphic InGaAs quantum well active region produces enough gain and good electrical confinement leading to low-threshold current and high quantum efficiency [2,3]. Technology of growth of SCH SQW structures has been developed to practical measures due to ours previous experiences with AlGaAs/GaAs semiconductor lasers fabricated at the Institute of Electron Technology [4,5]. Development of technology of strained layer InGaAs/GaAs structures was an obvious step further.

## 2. Laser design and above threshold analysis

The laser structures were designed for 980-nm operation at room temperature (T = 300 K). The required wavelength can be obtained by adjusting In content in the active layer and the thickness of the quantum well. Assuming ~20% In content in InGaAs QW, the thickness of the quantum well has been estimated roughly to be in the range between 60 Å and 100 Å to give the emission in the 980-nm range. This has been generally verified by PL measurements on the grown test structures. The lasing wavelength of the electrically pumped device, however, differs slightly from PL, since at the high injection conditions we deal with two contradictory effects; band filling and bad gap renormalisation (shrinkage) due to many body, Coulomb interactions in dense electron and hole plasma. Therefore, for proper design of the laser it is necessary to perform full simulation of the above threshold operation of the device which includes all relevant physical phenomena. Simulation has been performed using commercial PICS 3D software package [6]. Typically, besides emission spectra, P-I (optical power-current) characteristics for lasers with stripe contact and different resonator lengths are calculated. The calculated threshold current densities have to be understood as a bottom limit; in actual devices one should expect the higher values, due to unavoidable technological and processing faults and inaccuracies. Numerical simulation gives us guidelines for designing lasers and optimising they perfor-

*e-mail: bugajski@ite.waw.pl

mance and speeds up development of practical devices. Since laser performance optimisation has to be subjected to numerous restrictions (material and technological the numerical modelling is indispensable tool saving many efforts which would be otherwise spent on technological experiments.

## 2.1. Physical basis of laser simulator

Basic equations describing operation of semiconductor laser are Poisson's equation

$$-\nabla(\frac{\varepsilon\varepsilon_0}{e}\nabla V) = -n + p + N_D(1 - f_D) - \\ - N_A f_A + \sum_j N_{tj}(\delta_j - f_{tj}) \quad , \qquad (1)$$

and continuity equations for electrons and holes

$$\nabla J_n - \sum_j R_n^{tj}, - R_{sp} - R_{st} - R_{au} = \frac{\partial n}{\partial t} + N_D \frac{\partial f_D}{\partial t}, \qquad (2)$$

$$\nabla J_p + \sum_j R_p^{tj} + R_{sp} - R_{st} + R_{au} = -\frac{\partial n}{\partial t} + N_A \frac{\partial f_A}{\partial t}. \qquad (3)$$

The above equations govern electrical characteristics of the device (e.g., I–V characteristics). Analysis of the optical characteristics requires solution of Helmholtz equation, describing optical field distribution in the resonator

$$\nabla^2 W + k_0^2(\varepsilon - \beta^2)W = 0. \qquad (4)$$

The densities of electron and hole currents $J_n$ and $J_p$ can be expressed as a function of free carrier concentrations and variations of respective quasi-Fermi levels

$$J_n = n\mu_n \nabla E_{fn}, \qquad (5)$$

$$J_p = p\mu_p \nabla E_{fp}. \qquad (6)$$

Laser simulator solves self-consistently the above set of partial differential equations for the electrostatic potential V, electron and the hole concentration n and p, the optical field distribution W and the photon number in the resonator S. For the analysis of semiconductor laser it is important to evaluate the carrier density and the optical gain of a quantum well. The standard approach to the modelling is based on the parabolic band model. It is the most efficient model and usually it reproduces the general trends with satisfactory accuracy. For more accurate calculations, especially in the case of strained layer InGaAs/GaAs lasers one has to relay on more elaborate models. Inclusion of the biaxial strain in the design of quantum well semiconductor lasers provides an additional degree of freedom and produces some desirable effects, such as lower threshold current. The effects of strain are described theoretically using **k.p** description of the band structure in the quantum well. This type of calculation up to now has limited capability in analysing practical design issues and optimisation of laser geometry. The approximate treatment of the strain is based on the approximation of non-parabolic band structure by an anisotropic parabolic one [with proper inclusion of strain-induced shifts and splitting of light hole (LH) and heavy hole (HH) bands]. The calculations are based on analytical approximation to the band structure of strained quantum well, which has recently been developed [7] using an efficient decoupling method to transfer the 4×4 valence band Hamiltonian into two blocks of 22 upper and lower Hamiltonians. As a result of the decoupling, analytical expressions for in plane valence sub-bands dispersion relations can be derived. Once the parabolic subbands are found, one can apply conventional approaches to treat carrier concentration and the optical transition probabilities. The effective mass perpendicular to the quantum well plane determines the quantum sub-band energies at $\mathbf{k} = 0$, while the densities of states for each sub-band are determined using the in plane effective masses. In the framework of the model developed in [7] it is also possible to account for anti-crossing behaviour of the valence band sub-bands (i.e., valence band mixing).

With no carrier injection the active layer material is strongly absorbing. With carrier injection we can invert the carrier population near the band edge and convert absorption into gain. The region of positive gain exists in limited energy range above the bandgap of the material. It extends between the bandgap and the quasi-Fermi level separation: $E_g < h\nu < \Delta E_g$. The spectral shape of the QW gain and peak gain on injected carrier density expressions differ considerably from that of bulk material. These differences are the consequences of the step-like density of states in QW material. Apart from this, the derivation of appropriate expression for gain follows usual treatment. The optical gain is calculated using standard perturbation theory (Fermi's Golden Rule). The spectrally dependent gain coefficient can be written in the form

$$g(E) = \frac{q^2|M|^2}{E\varepsilon_0 m^2 c\hbar N L_z} \\ \times \sum_{i,j} m_{r,ij} C_{ij} A_{ij} [f_c - (1 - f_v)] H(E - E_{ij}) \qquad (7)$$

where $|M|^2$ is the bulk momentum transition matrix element; $C_{ij}$ is the spatial overlap factor between states i and j, $A_{ij}$ is the anisotropy (polarisation) factor for transition i,j; $m_{r,ij}$ is the spatially weighted reduced mass for transition i,j; $E_{ij}$ is the transition energy between states i and j; N is the effective refractive index; H is the Heaviside step function; i, j is the conduction, valence (lh, hh) quantum numbers at Γ point. For the perfectly confined QW states $\Delta n = 0$ selection rule applies. The reduced mass parameter is

 

given by $m_{r,ij}^{-1} = m_i^1 + m_j^{-1}$, where $m_i$ and $m_j$ are weighted (by wavefunction confinement factor in QW) averages of QW and cladding masses.

Momentum conservation restricts the energies of the initial and final states. The bulk averaged momentum matrix element between the conduction and valence states is

$$|M|^2 = \frac{m^2 E_g (E_g + \Delta)}{6 m_c (E_g + 2\Delta/3)}. \tag{8}$$

The angular anisotropy factor is normalised so that its angular average (bulk limit) is unity. For the TE transitions, with the electric field vector in the plane of the QW, its values are: $A_{ij} = 3/4(1+\cos^2\theta_{ij})$ for e-hh transitions and $A_{ij} = 1/4(5-3\cos^2\theta_{ij})$ for e-lh transitions. The bands are assumed to be parabolic in first approximation, thus the occupation density of the i-th (conduction or valence) band is

$$n_i, p_i = \frac{kT m_i^{c,v}}{\pi\hbar^2 L_z} \ln\left[1+\exp\left(\frac{E_f^{c,v} - E_i^{c,v}}{kT}\right)\right] \tag{9}$$

where the quasi-Fermi energies $E_f$ and the quantum levels $E_i$ are measured positive into respective band from the k = 0 band edge. We assume undoped QW with high injection, so the charge neutrality gives the condition $n = p_{lh} + p_{hh}$. The carrier scattering processes are accounted for by introducing appropriate broadening of the quantum levels. The net effect of this broadening can be found by convoluting the Lorentzian shape function with gain distribution [$g'(E) = g(E) \times L(E)$]. The broadening significantly reduces the local gain. The discussed relations allow for calculating gain vs. injected carrier density.

The above equations give the material gain of quantum well in terms of carrier density, which is not directly measurable. From the point of view of calculating properties of semiconductor injection laser the relation between the current and carrier density must be established by balancing current with total carrier recombination rate which consists of radiative and nonradiative components. The radiative component of carrier recombination is found from spectrally dependent spontaneous emission rate. The nonradiative contribution to the current comes mainly from thermal leakage current and from Auger recombination. The most common method of estimating Auger recombination is to use experimentally obtained Auger coefficients in combination with calculated carrier density ($R_A = CN^3$). Theories can predict Auger rate to within an order of magnitude. In quantum-well lasers carriers can leak into separate confinement waveguiding layers as well as leaking out of the entire SCH waveguide region into the doped cladding layers. Carrier population in the SCH region leads to recombination giving leakage current density of the order of 50 A/cm$^2$ per $10^{17}$ cm$^{-3}$ of carrier density. This shows the importance of maintaining low carrier density in the waveguide regions of the laser.

The theory of gain based on Fermi's Golden Rule considers each electron in isolation as it interacts with electromagnetic field, i.e., it is a single-particle theory and as such it neglects mutual interactions between electrons. The physical consequences of many-body effects in dense electron plasma in QWs are basically of two types: excitonic effects and bandgap renormalisation effects. The first one will result essentially in the changes of the spectral shape of material gain curves and will be enhanced in quantum wells comparing to the bulk material. The second will produce the bandgap shrinkage due to the combined exhange and correlation effects. The net effect of the bangap shrinkage is the noticeable red-shift of gain spectrum accompanied by its reshaping and enhancement. This phenomenon is clearly observable in quantum well lasers where the high threshold carrier density shifts the lasing wavelength beyond the known band edge wavelength of the quantum well. Nevertheless, all practical laser simulators available now are based on free-carrier gain model, which is easier to implement numerically. The full account of many-body laser theory can be found in the monograph [8].

## 2.2. Numerical simulation of SCH SQW InGaAs/GaAs laser

The sketch of the typical device simulated is shown in Fig. 1. The sequence of layers consists of n-type GaAs buffer, the $Al_xGa_{1-x}As$ n-type barrier layer, undoped active layer and waveguide, the $Al_xGa_{1-x}As$ p-type barrier layer and $p^+$-type GaAs sub-contact layer. Active layer is composed of $In_yGa_{1-y}As$ quantum well enclosed by GaAs waveguide. The model was tested for different values of structure parameters, i.e., thickness of individual layers, composition and doping. The indium content in InGaAs QW was varied from y = 0.20 to y = 0.22 and the well thickness from 60 Å to 100 Å. The AlGaAs compositions x = 0.30 and x = 0.70 were tested. Finally, we have studied the influence of the thickness of GaAs waveguide, which had been changed from 0.1 μm on each side of QW to 0.3 μm, on the laser characteristics. The doping of both emitters was kept on $5\times10^{17}$ cm$^{-3}$ level for all simulations. Such complex program of investigations would be difficult to realise by relaying exclusively on technological experiments. Nevertheless, the key numerical results were confronted with real experiments to verify calculations and provide solid foundations for hypothesis derived from numerical experiments. Such combined approach proved to be very successful in developing 980-nm lasers.

Typical, calculated P-I (optical power-current) characteristics for lasers with stripe width W = 100 m and resonator length L = 700 μm are shown in Fig. 2. Threshold current densities for modelled lasers are equal to 197 A/cm$^2$ and 208 A/cm$^2$, depending on construction details, which are in agreement with values obtained experimentally by

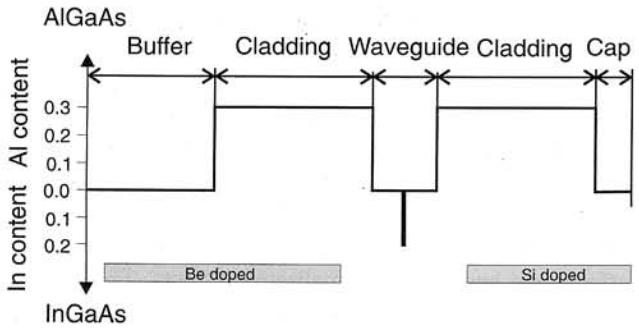


Fig. 1. SCH SQW InGaAs/GaAs strained layer laser structure.

Coleman [2] for broad area strained-layer InGaAs/GaAs lasers of similar geometry but wit higher Al content in the emitters. The majority of early lasers were GRIN SQW type, while now simple SCH SQW lasers, as studied in this work, dominate, which in most cases makes comparison of calculated results with available experimental data only approximate, but general trends are reproduced properly. The calculated threshold current densities have to be understood as a bottom limit; in actual devices one should expect the higher values, due to unavoidable technological and processing faults and inaccuracies. Figure 3 illustrates the results of the simulation of spectral characteristics of mentioned lasers. Shown are the spectra of longitudinal modes belonging to the fundamental transverse and lateral mode. Due to the discrete nature of quantum well thickness variations, which are expressed as integer multiples of monolayers (1 ML = 2.83 Å) to get required emission wavelength one has to vary both QW thickness and In composition at the same time.

Application of narrower waveguiding layer (~0.1 μm on each side of the quantum well) decreases threshold current by about 25% (cf. Fig. 4) but on the other hand optical power density in the resonator increases roughly 3 times. This may lead to a faster degradation of lasers, in particular to the lowering of catastrophic optical damage (COD) threshold level. The heat generated by the absorption of laser radiation at the mirrors can result in irreversible damage of the laser. Since our primary concern was durability of lasers the former design, with broader waveguide, was chosen although the penalty of slightly higher threshold had to be paid. Extremely low threshold current densities, of the order of 120 A/cm$^2$, can be obtained using both narrow waveguide (~0.1 μm) and high Al content (x = 0.70) in the emitters. Such construction can be useful for low power, high-speed lasers with narrow stripes (5 μm–10 μm) operated at low drive currents.

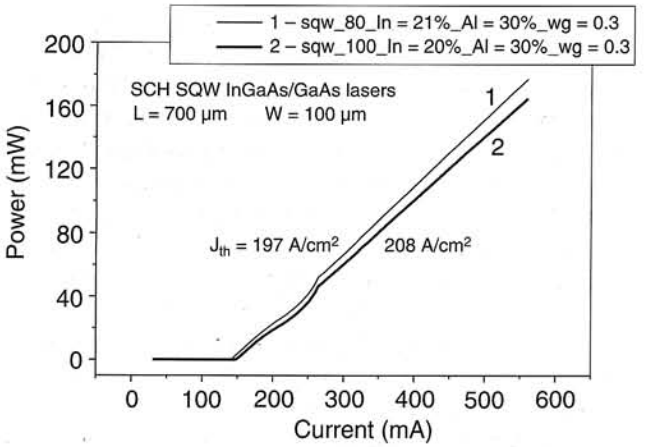


Fig. 2. Calculated P-I characteristics of SCH SQW InGaAs/GaAs lasers.

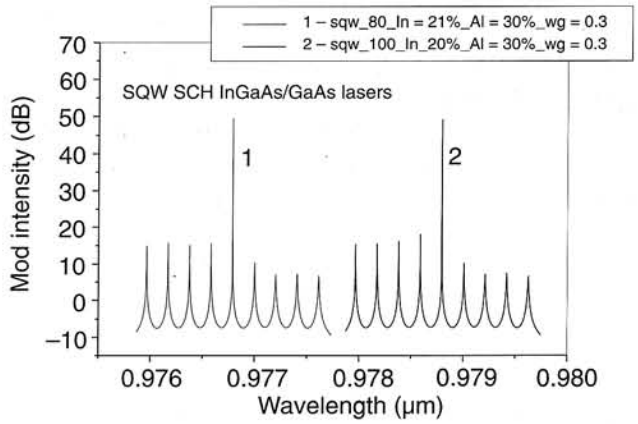


Fig. 3. Calculated spectral characteristics of SCH SQW InGaAs/GaAs lasers.

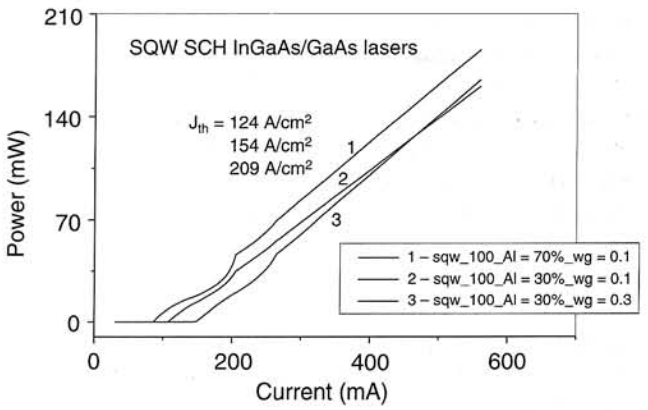


Fig. 4. Calculated P-I characteristics of SCH SQW InGaAs/GaAs lasers (different waveguide parameters).

The influence of QW thickness, with the other construction details unchanged, on laser parameters has been also studied. The results of calculation are shown in Fig. 5. The differential quantum efficiency of the laser (η) grows with decreasing QW thickness, reaching 0.54 W/A (42.7%) for L = 60 Å. On the other hand, the threshold current density $J_{th}$ reaches minimum 121 A/cm$^2$ for L = 80 Å. The reported results suggest that a good optimisation procedure would be to choose QW thickness L = 80 Å and vary In content in the active region to get required wavelength of laser emission, i.e., 980 nm. The thickness of both emitters should be at least 1.0 μm each, preferably 1.5 μm, to assure

 

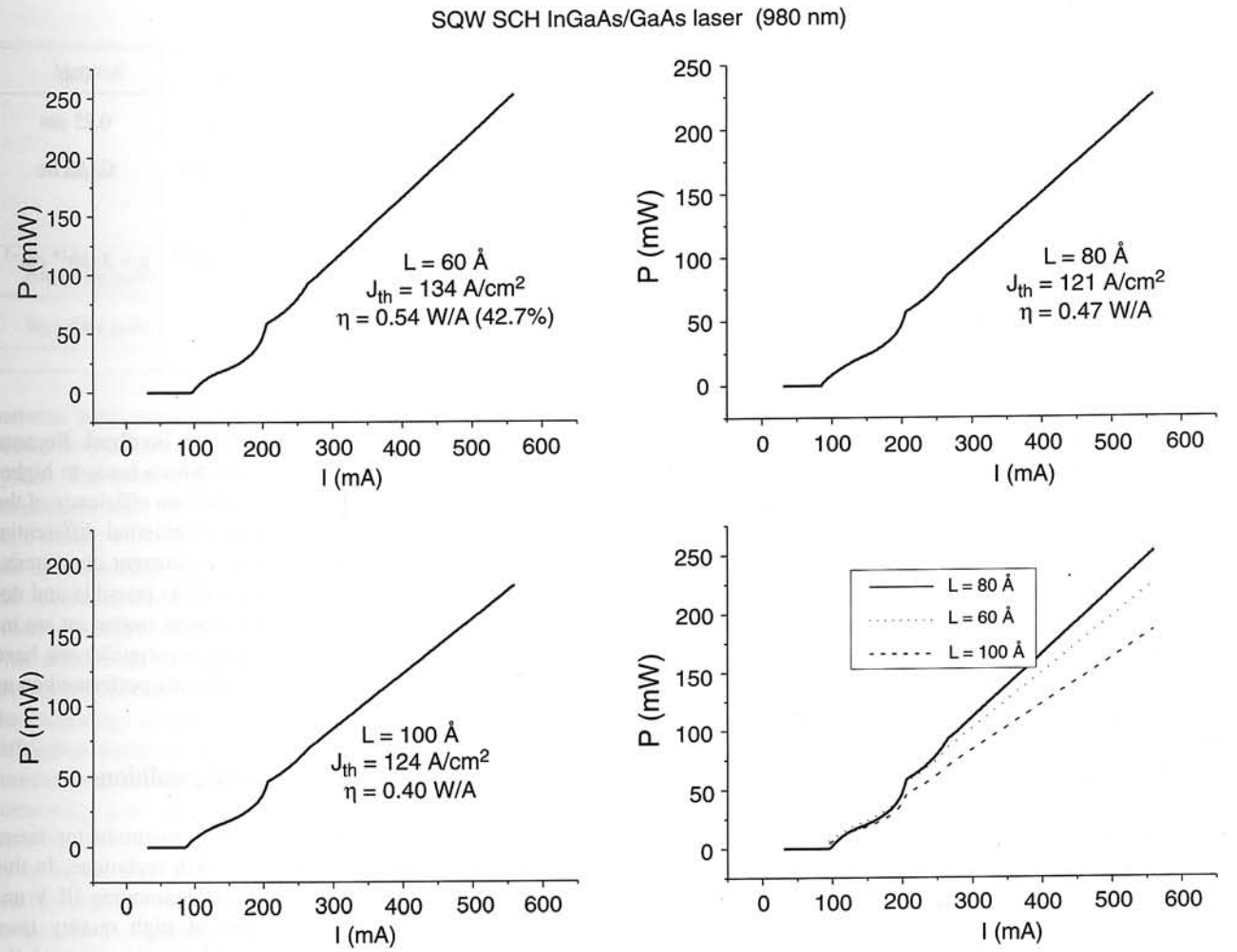


Fig. 5. Calculated P-I characteristics of SCH SQW InGaAs/GaAs lasers (different QW thickness).

that optical field of the fundamental mode does not penetrates the highly absorbing GaAs regions.

The final laser structure has been decided according to the simulation results. The thickness, composition and doping of individual layers constituting the structure were chosen as listed in Table 1. SCH SQW laser structures were grown by molecular beam epitaxy (MBE) in Riber 32P reactor in a manner similar to the previously described in Ref. 9. The structures were grown on (100) GaAs conductive substrates. The sequence of layers for typical optimised for reliable high power CW operation structure consisted of n-type GaAs buffer, the $Al_{0.3}Ga_{0.7}As$ n-type barrier layer, undoped active layer and waveguide, the $Al_{0.3}Ga_{0.7}As$ p-type barrier layer and $p^+$-type GaAs subcontact layer. Active layer and waveguide comprised of $In_{0.21}Ga_{0.79}As$ 80 Å quantum well enclosed by 0.3 μm GaAs layers.

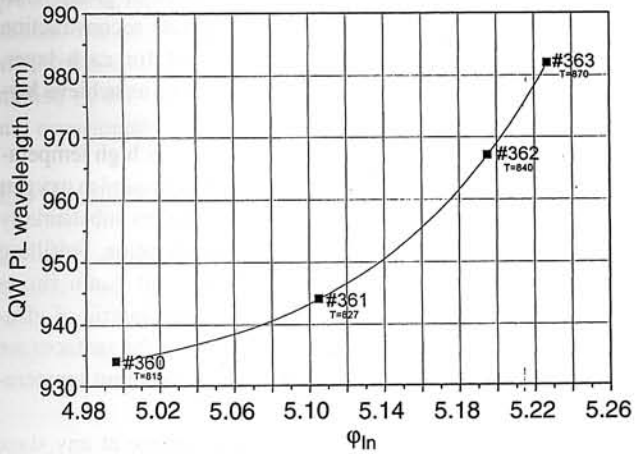


Fig. 6. PL wavelength from InGaAs/GaAs laser structure as a function of indium flux $_{In}$ (calibration curve).

## 3. Strained-layer laser structures – MBE growth related issues

The growth of InGaAs/GaAs heterostructures is much more difficult than the growth of AlGaAs/GaAs ones. The reason for that is large lattice mismatch between substrate and the growing layer. The lattice constant of GaAs is equal to 5.6533 Å, whereas that of InAs equals 6.0584 Å, which results in 7% lattice mismatch between those two semiconductors and precludes the growth of high indium containing InGaAs

Table 1. Typical parameters of SCH SQW InGaAs/GaAs/AlGaAs laser structures.

| Buffor | n-emiter | Waveguide | QW | Waveguide | p-emiter | Cap |
|---|---|---|---|---|---|---|
| 1 μm GaAs:Si | 1–1.5 μm | 0.1–0.3 μm | 80 Å | 0.1–0.3 μm | 1–1.5 μm | 0.25 μm |
| $n = 2\times10^{18}$ cm$^{-3}$ | $Al_xGa_{1-x}As$:Si | GaAs | $In_xGa_{1-x}As$ | GaAs | $Al_xGa_{1-x}As$:Be | GaAs:Be |
| 0.2 μm | x = 0.3 | | x = 0.20–0.22 | | x = 0.3 | |
| $Al_xGa_{1-x}As$:Si | $n = 5\times10^{17}$ cm$^{-3}$ | Undoped | Undoped | Undoped | $p = 5\times10^{17}$ cm$^{-3}$ | $p = 3\times10^{19}$ cm$^{-3}$ |
| x = 0.0–0.3 | | | | | | |
| $n = 5\times10^{17}$ cm$^{-3}$ | | | | | | |

on GaAs substrate. The room temperature band gap of $In_xGa_{1-x}As$ ternary alloy varies from 1.424 eV (GaAs) to 0.36 eV (InAs). The energy range close to 1.424 eV is attainable by using $In_xGa_{1-x}As$ layers grown on GaAs substrates. This way the layers with indium content up to 0.2 and reasonable thickness up to 100 Å can be grown [10]. The layer with different lattice constant than that of the substrate undergoes a tetragonal deformation during the growth. Depending on whether the lattice constant of the layer is greater or smaller than the lattice constant of the substrate, we have biaxial compressive or biaxial tensile strain in the plane of the layer and appropriate deformation of the elementary lattice cell in perpendicular direction for which the strain is relaxed. With increase of the layer thickness, the elastic deformation energy stored in the crystal grows and when its value exceeds certain threshold value determined by the Hook's law the stress is released and the misfit dislocations are formed [11]. The thickness of the layer for which stress relaxation occurs is called a critical thickness. It depends mainly on the lattice mismatch between the layer and the substrate. For the materials with large lattice mismatch, such as InGaAs on GaAs, the critical thickness values are few orders of magnitude smaller than that for AlGaAs on GaAs with a similar composition. The lattice mismatch is the main factor responsible for difficulties encountered in the growth of InGaAs on GaAs. The growth of lattice mismatched layers can be realised only in the limited range of thickness and compositions and even then is a difficult task, requiring a precise knowledge of the phenomena occurring in strained materials.

Band structure of III-V semiconductor compounds changes appreciably under biaxial strain originating in thin layers of these materials grown on lattice mismatched substrates. The presence of strain removes degeneration of valence band k = 0, changes band gap as well as dispersion relation in the valence band. In quantum wells the influence of strain is even more complicated. All these changes can be positively exploited in designing quantum well lasers, resulting in improved device characteristics and flexibility in fabricated lasers parameters [12]. Penalty paid for this is difficult growth technology. Quality of interfaces and defects in strained layer semiconductor structures greatly affect parameters of lasers. Roughness of surfaces is cause of dissipative loss of emission and probable non-radiative recombination on defects involved. Because of that total internal losses increase which leads to higher threshold current and decrease of quantum efficiency of the lasers. This finally causes decrease of external differential efficiency (slope of optical power vs. current characteristics is smaller). To achieve as smooth as possible and defect free interfaces (in particular the most important are interfaces between quantum well and waveguide) we have applied photoluminescence measurements performed on as grown structures [13].

## 3.1. Optimisation of MBE growth conditions

The performance and reliability of semiconductor lasers depends critically on the crystal growth technique. In this respect, lasers are probably the most demanding III-V minority carrier devices. Fabrication of high quality laser structures by MBE needs a careful optimisation of the growth conditions. From the point of view of MBE technology several factors are of great importance: high purity and structure perfection of undoped layers, the relevant profiles of dopant concentration, good quality of interfaces, high dopant concentration in contact layers, etc. Therefore, the optimisation of the MBE process comprises the determination of the growth conditions for each layer of the laser structure. The growth must proceed with right combination of temperatures of substrate and ratios of group V/III atomic beams, which guarantee appropriate reconstruction of surface and proper growth conditions for each layer, which indeed vary appreciably. This allows us achieve layers of the best optical quality.

In general AlGaAs should be grown at as high temperatures as possible and at low V/III ratio (to minimise oxygen content in the layers), whereas InGaAs prefers substantially lower temperatures and higher V/III beam ratios. Fulfilling these conditions requires abrupt changes of beam fluxes which is difficult to realise due to thermal inertia of effusion cells. To avoid process interruptions at the surfaces we have used two arsenic cells preheated at different temperatures.

To monitor the state of the crystal surface at any stage of the growth process the RHEED (reflection high-energy electron diffraction) system was used [14]. The RHEED

 

Table 2. Optimised MBE growth conditions for InGaAs/GaAs laser structures.

| Material | Layer | T (°C) | Growth rate (μm/hr) | V/III flux ratio | Reconstruction |
|---|---|---|---|---|---|
| GaAs | Buffer | 580 | 0.8 | 4–5 | (2×4) |
| | Waveguide | 550–580 | | | |
| | Subcontact | 540 | | | (3×1) |
| $Al_{0.30}Ga_{0.70}As$ | Emitters | 690 | 1.15 | 2.1 | (3×1) |
| $In_{0.20}Ga_{0.80}As$ | QW | 550 | 1.0 | 4 | (2×4) |

patterns were registered by CCD camera and then processed in real time and recorded by a computer acquisition system. The system enabled us to register RHEED intensity oscillations and, as a result, to determine the growth rate. As a result, we had at our disposal two independent methods of measuring the growth rate. The first one based on the measurement of atomic fluxes and the second one based on registering the RHEED intensity oscillations. That additional possibility strengthened our control over growth process and turned out to be crucial in developing the technology of laser structures. The analysis of RHEED diffraction patterns allowed us to determine substrate reconstruction for the case of growth of different materials composing laser structure, depending on the temperature and respective beam fluxes. It is well known that the quality of layers and their usefulness for certain applications can be linked to the type of surface reconstruction during the growth. For GaAs there are known types of reconstruction which produce layers especially suitable for optical applications. In the case of InGaAs the subject is less studied but the general trends are similar. Based on our previous experiences with GaAs/AlGaAs system and research done for this work we have found the set of optimum growth conditions (in terms of beam fluxes, surface reconstruction and temperatures) for the growth of InGaAs/GaAs/AlGaAs strained layer structures. They are listed in Table 2.

Optimised MBE growth parameters allowed for the growth of defect free laser structures in the whole range of indium content in the active region studied (0.10–0.25 mole fraction of In). Quality of the structures was routinely studied by PL (photoluminescence), PR (photoreflectance) and occasionally by TEM.

### 3.2. Optimisation of emission wavelength

The erbium-doped fibre amplifiers (EDFAs) coherently amplify 1550-nm signals through the conversion of 980 nm pump laser light. To assure efficient pumping the wavelength of the laser should be 980 ±5 nm. This requirement imposes certain limits on technology of the structures. The emission wavelength of the laser is determined by the geometry of the QW active region (the well thickness and depth). The precision of thickness control in MBE method is much higher than ability to control composition of individual layers. That results mainly from the fact than in the first case one can use RHEED oscillations to monitor single monolayer deposition, whereas composition of the layers is determined by the respective beam fluxes, which in turn are controlled by the effusion cell temperatures; process prone to inaccuracies. Additionally the QW composition changes allow for continuous tuning of the wavelength whereas the changes of QW thickness are by the nature discrete ones. From the theoretical modelling of laser one can conclude that the optimum thickness of QW is 80–100 Å and its composition 20–21%. Therefore the following methodology has been adopted to achieve required emission wavelength of 980 nm (or at least to get close to it). The thickness of the quantum well was set to 80 Å and the series of growth processes has been performed for different values of indium flux $\varphi_{In}$ with the remaining growth parameters kept unchanged. The emission wavelength for each structure has been subsequently determined by photoluminescence (PL). The result was a calibration curve relating emission wavelength with easily controllable indium flux measured in relative units. The changes of In cell temperature from 815°C to 870°C result in emission wavelength changes from 935 nm to 985 nm and character of observed changes is monotonic, which gives us an effective technological means to control emission wavelength with required accuracy. The calibration holds as long as the growth chamber is not opened for maintenance. After the opening the chamber the growth process should be re-calibrated, at least partly. The experience tells us, however, that usually 1 or 2 growth processes are required to regain a full control over the reactor.

## 4. Wafer characterisation of laser structures

The epitaxial wafers before being subjected to further processing have to be nondestructively characterised in order to determine whether they meet specification dictated by the applications. The experimental technique, particularly useful in that case is PL mapping [15]. Besides the intensity of luminescence, which is a measure of overall sample quality, the wavelength of the QW emission should be measured in each case. The precise wavelength control is an essential prerequisite for successful 980-nm laser fabrication. Whereas the general

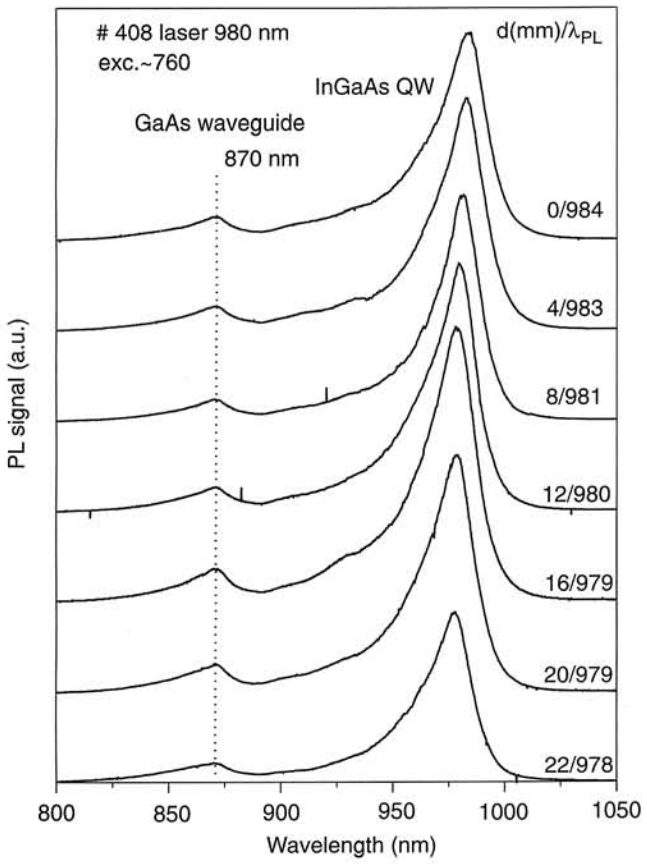


Fig. 7. PL spectra from InGaAs/GaAs laser structure recorded at different points along the wafer diameter.

tuning of the wavelength can be achieved, as described earlier, by the adjustment of In flux, while growing the active QW, the inadvertent wavelength nonuniformities over the wafer still exist. They primary cause is a spatial nonuniformity of molecular (atomic) beams emitted from effusion cells. These nonuniformities can be minimised within reasonable limits but being connected with the very nature of effusion process as well as construction of growth chamber they can not be completely eliminated. The measurements of spatially resolved photoluminescence, performed on grown wafers show that wavelength variations over the 2" wafer radius can be as large as 5–8 nm (see for example Fig. 7). The characteristic wavelength variations observed on wafers have circular symmetry as it can be deduced from the PL intensity maps shown in Figs. 8 and 9. The maps were taken for fixed detection wavelength and PL intensity changes can be directly linked to detuning of the emission wavelength and detection wavelength. Assuming that wavelength tolerance required by laser is ±3 nm, practically the whole wafer #408 (cf. Fig. 7) fulfils the set criteria. In the case when wavelength variation over the wafer exceed set limits one can at least select parts of wafer, which are suitable for further processing. The PL maps provide direct information about wafer uniformity and allow for fast and efficient inspection before processing them into the laser chips. As a control method the technique of PL mapping can be hardly replaced by anything else.

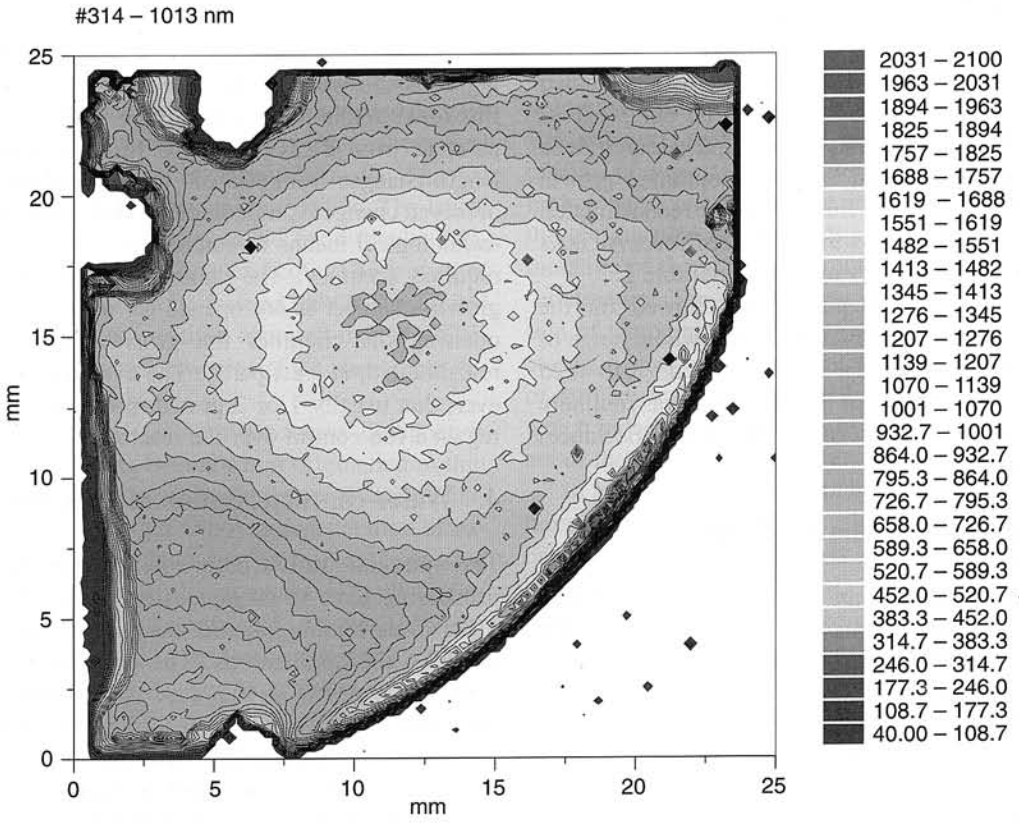


Fig. 8. PL intensity map for ¼ of 2" wafer with InGaAs/GaAs laser structure (PL emission originates from QW).

 

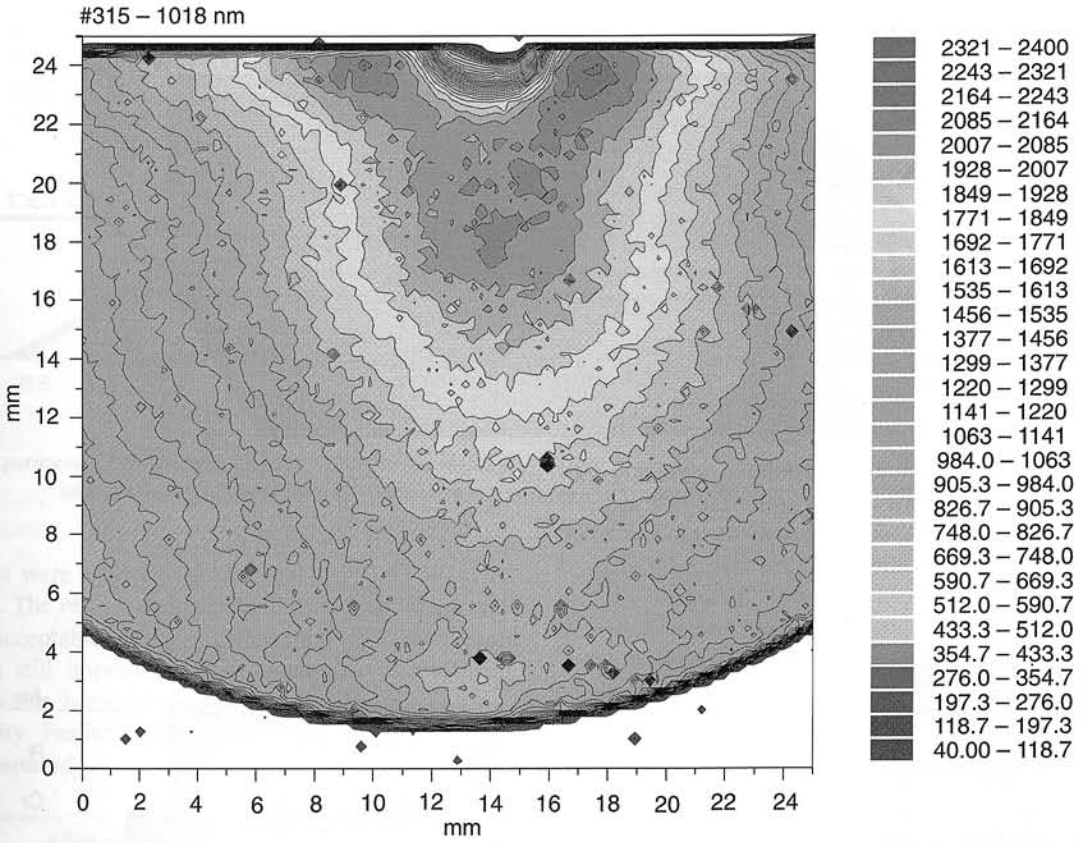


Fig. 9. PL intensity map for ½ of 2" wafer with InGaAs/GaAs laser structure (PL emission originates from QW).

## 5. Device fabrication and laser characteristics

The broad contact (100-μm stripe width) ridge-waveguide lasers were fabricated from SCH SQW structures following a standard processing procedures used previously for DH AlGaAs/GaAs lasers. The schematic view of the laser structure, with magnified details of active region, is shown in Fig. 10. The AuGeNi/Au contact with additional thick Au layer was used for n-side of the device. The p-contact comprised of the following sequence of layers: Cr (50 nm), Pt (200 nm), Cr (50 nm) and Pt (150 nm). The individual lasers were In-soldered, p-side down, on copper blocks (see Fig. 11) and contacted by a gold wire. The p-side down soldering of lasers has an advantage over n-side down mounting manifesting in better heat sinking, although it is much more difficult technologically and generally results in lower yield. The top view of the contact pad of a two-segment (2×350 μm) laser with the 100-μm wide stripe is shown in Fig. 12. The laser resonators with different length can be realised by taking different number of segments. All laser chips were tested before soldering, using needle probe and micromanipulator. The P-I characteristics and spectral characteristics were measured. The CCD camera was used to observe near-field picture of laser emission. Light from the laser was delivered to the spectrometer using optical fibre. The measurements of laser characteristics, data acquisition, and data processing were controlled by PC computer. For selected devices angular distribution of laser emission in two perpendicular directions (far-field pattern) was also recorded. Finally, devices were encapsulated in metal cases with window. Some of the lasers had antireflection (AR) and high-reflectivity (HR) coatings deposited on the front and rear facets respectively. One layer of $SiO_2$ was used for AR coating and $Si/SiO_2$ multilayer was used for HR-coating. The AR, HR coatings were deposited on lines of lasers, before dividing them into individual chips.

The preliminary results of the works on 980-nm lasers have been published in series of recent papers of the authors [16–19]. Here we report updated results on degradation studies and selected best characteristics of the lasers. The progress in the technology of the 980-nm lasers observed in recent months was so marked that some results of our papers published in last year are already partly outdated. To give an example, we have managed to lower the threshold current of the lasers by more than twice in a year time and improved their reliability by more than order of magnitude.

Fabricated lasers exhibited similar characteristics to the other structures of this type published in the literature [20–24]. Threshold current densities of the order of $J_{th}$ = 280 A/cm$^2$ (for the resonator length L = 700 μm) and differential quantum efficiency $\eta$ = 0.40 W/A (41%) were obtained. The wall-plug efficiency of the lasers without AR coating reached 38%. The typical optical power-current characteristics (P-I) for group of lasers fabricated from the

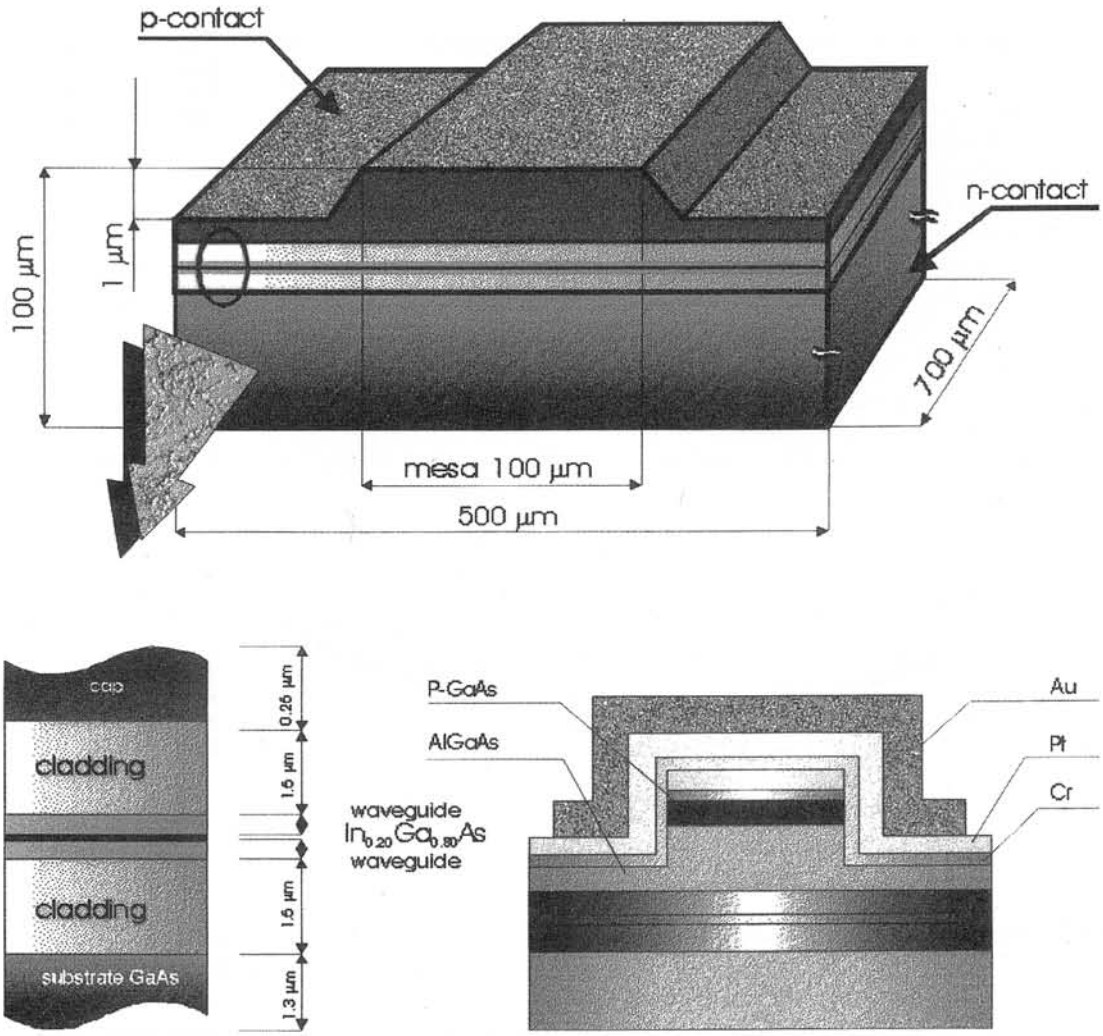


Fig. 10. The schematic view of the laser chip, with magnified details of active region.

on wafer are shown in Fig. 13. They show almost equal thresholds and slightly different differential efficiencies. The linearity of the characteristics is good; there is no kinks and thermal roll-over for highest powers observed. The characteristics refer to pulse operation with filling factor ff = 0.1% (pulse length 200 ns, repetition 5 kHz).

Theoretical estimation of threshold current density and differential efficiency obtained by numerical modelling of

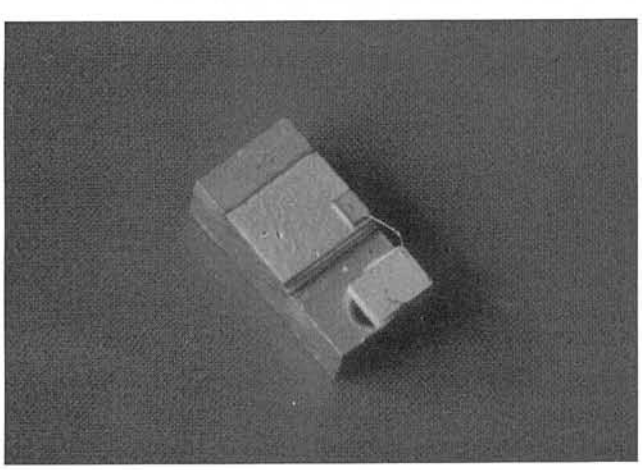

Fig. 11. Laser In-soldered p-side down on copper blocks and contacted by a gold wire.

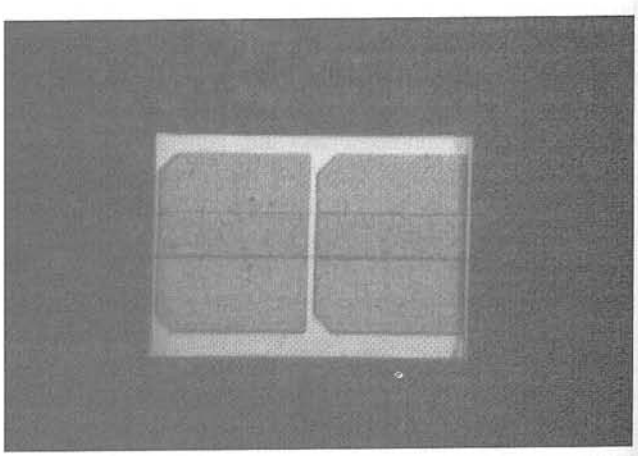

Fig. 12. Top view of the laser chip formed by two segments of the length 350 µm each (notice the stripe of the width of 100 µm in the middle of the contact pad).

 

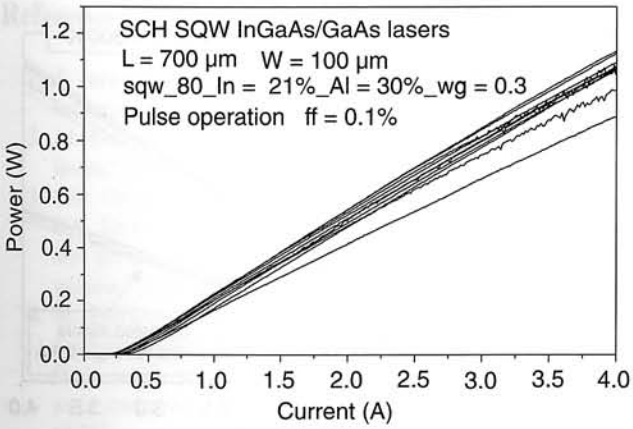


Fig. 13. Experimental ight-current characteristics of SCH SQW InGaAs/GaAs/AlGaAs lasers.

the devices were $J_{th}$ = 210 A/cm$^2$ and $\eta$ = 0.47 W/A, respectively. The obtained experimentally threshold currents are fully acceptable, whereas differential efficiency could have been still improved. They lower than theoretically predicted value is most probably caused absorption losses in the cavity. Further work aimed on lowering absorption losses is required.

The lasers generated at 980–990 nm wavelength range, depending on the part of the wafer from which they have been made, with the halfwidth of the emission band of the order of 1nm, just above the threshold and up to 3 nm at high currents (high optical power). Emission spectrum contained many well-distinguished longitudinal modes, belonging to the fundamental transverse and lateral modes. The typical spectral characteristics of developed lasers, for supply current 1.5 $I_{th}$ are shown in Fig. 14. These are to be compared the spectrum for current 5 $I_{th}$ shown in Fig. 15, which contains more longitudinal modes and exhibits appreciable thermal broadening. As it has been mentioned earlier the requirement of precise wavelength control demanded by application of the devices as a pump source for $Er^{3+}$-doped amplifiers is difficult to fulfil but manageable. Besides the variation of the wavelength over the wafer, there are global variations between different MBE runs. Usually, the best reproducibility is achieved when one grows a series of 2 "wafers with laser structures, without interruption for other processes. That assures a maximum stability of growth parameters.

To force laser emission through one, selected mirror one has to apply AR/HR coating. The other benefits of dielectric passivation of the mirrors is theoretically doubled

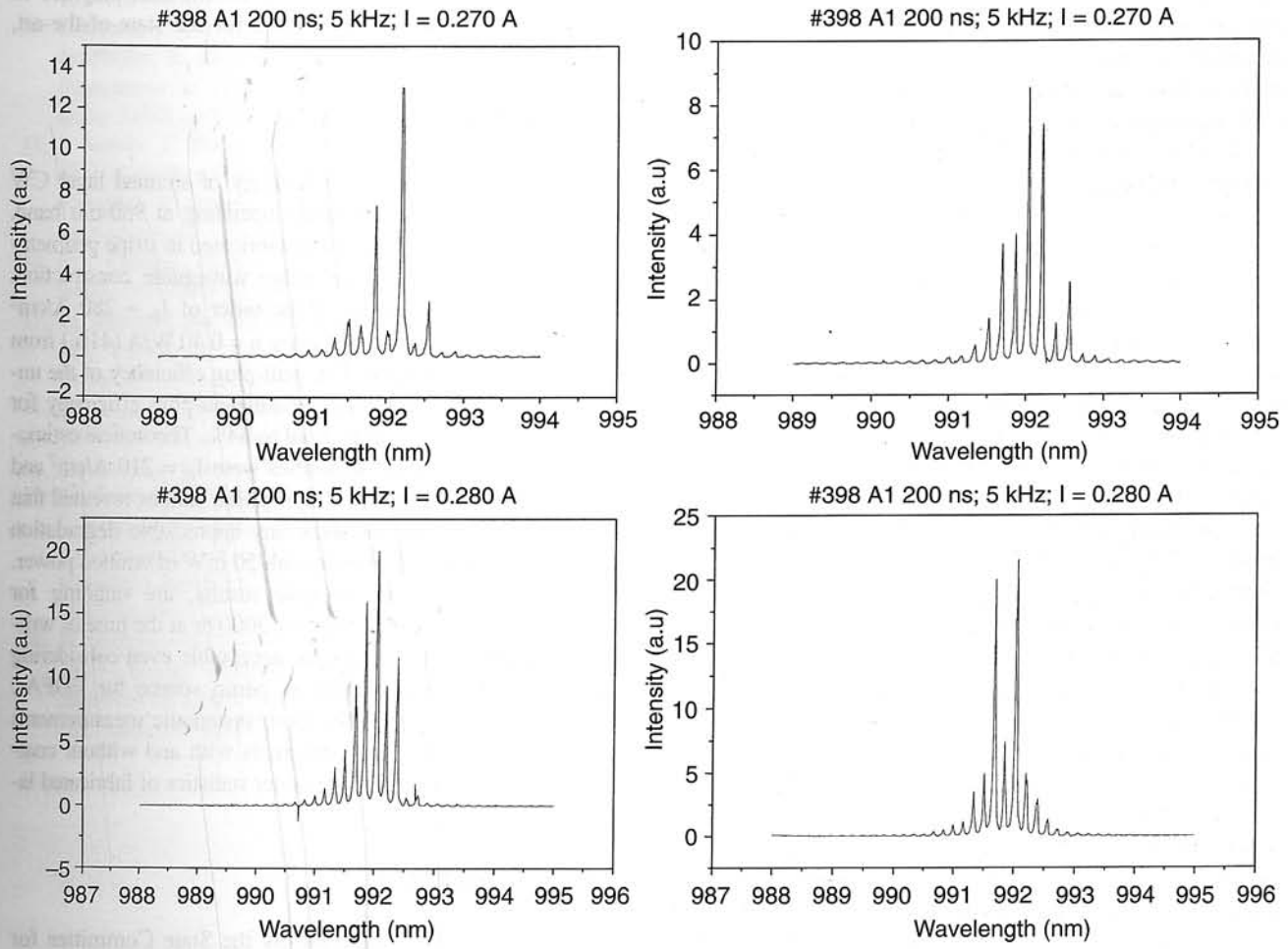


Fig. 14. Spectral characteristics of SCH SQW InGaAs/GaAs lasers (for currents just above the threshold I = 1.5 $I_{th}$).

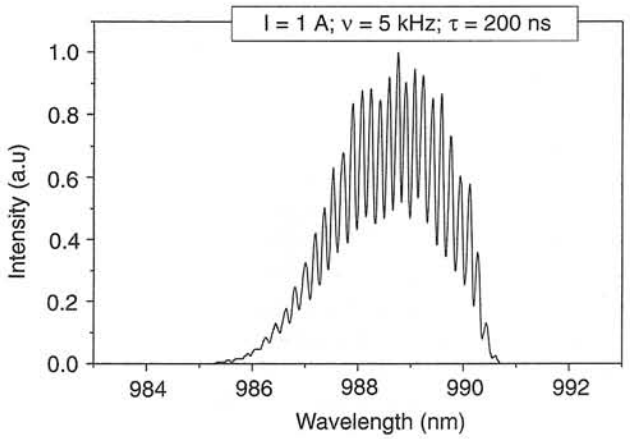


Fig. 15. Spectral characteristics of SCH SQW InGaAs/GaAs lasers (for high currents I = 5 $I_{th}$).

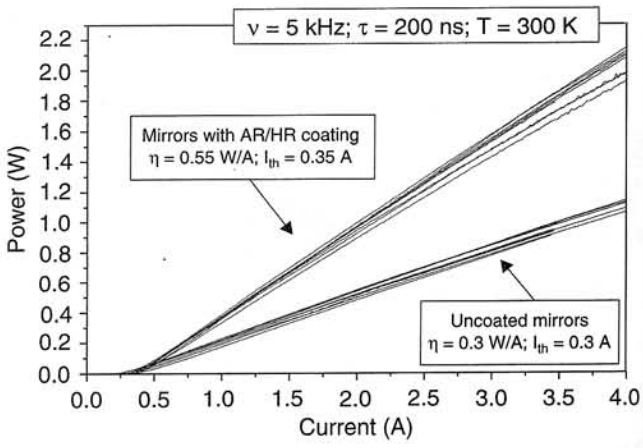


Fig. 16. Comparison of P-I characteristics of InGaAs/GaAs lasers with or without AR/HR coatings of the mirrors.

differential efficiency of the laser and higher resistivity to degradation. The last particularly refers to increased COD level and greatly enhanced durability. According to the recent reports [25], strained-layer InGaAs/GaAs lasers without mirror coating lived in CW regime on average about 250 hr, whereas the lifetime of those with AR/HR coatings reached 5000–10000 hr. Typical light-current characteristics of the lasers without AR/HR coatings and with AR/HR coatings, from one lot, are compared in Fig. 16. The threshold current of lasers with AR/HR coatings was unchanged comparing to uncoated ones but we have observed roughly twice increase in differential quantum efficiency. The record wall-plug efficiency for AR/HR coated devices was equal to 54%. Which is among the best values obtained for that type of lasers.

The yield of the final devices was satisfactionary. There were 40% lasers with good characteristics ($I_{th}$ < 400 mA) from among the population of the total 500 lasers fabricated and tested (at least as chips, before assembling)

For some lasers we have performed aging tests. The lasers for the tests were selected on the basis of initial screening based on threshold current determination. Only the lasers with threshold within the limit of up to twice the average threshold have been subjected to lifetime testing. No special effort was made to select particularly good devices, rather we tried to chose a spectrum of different initial quality devices. Fabricated lasers showed in general good reliability. The uncoated devices, did not show an appreciable degradation after over 1000 hr of CW operation at 35°C heat sink temperature, with 50 mW emitted power (in a constant power mode). This result can be extrapolated to $10^6$ hr of pulse operation with ff = 0.1%. In the light of the results published in literature [25] this is extremely good result, even having in mind that the lasers with whom we compare our results were operated at 100-mW optical power. A total of 10 devices were placed on life test. The lasers with coated mirrors are at the moment of writing this paper still operated at the aging frame and their CW working time reaches 1500 hr. Only one of them failed during the test and the rest maintan basically unchanged current. This is to be compared with typical CW operating times of a few khr published in the literature [26–28]. The apparent immunity of investigated lasers to sudden failure is striking and despite the small statistical base it undoubtfully an inherent property of strained-layer InGaAs/GaAs lasers as compared to conventional AlGaAs/GaAs lasers. Summarising the results of aging test performed so far and those, which are in progress, we may conclude that they are in agreement with the similar studies for the state-of-the-art, InGaAs/GaAs lasers.

## 6. Conclusions

We have developed MBE technology of strained layer CW InGaAs/GaAs SCH SQW lasers operating at 980-nm band. Broad contact, pump lasers were fabricated in stripe geometry using Schottky isolation and ridge waveguide construction. Threshold current densities of the order of $J_{th} \approx 280$ A/cm$^2$ and differential quantum efficiency $\eta = 0.40$ W/A (41%) from one mirror were obtained. The wall-plug efficiency of the uncoated lasers was 38%. The record wall-plug efficiency for AR/HR coated devices was equal to 54%. Theoretical estimation of above mentioned quantities were $J_{th} = 210$ A/cm$^2$ and $\eta = 0.47$ W/A respectively. Degradation studies revealed that uncoated devices did not show any appreciable degradation after 1000 hr of CW operation with 50 mW of emitted power. Similar life tests, with positive results, are ongoing for AR/HR coated devices already for 3000 hr at the time of writing this paper. These results are acceptable even considering such demanding applications as pump source for EDFAs. There is however a need for more systematic measurements in CW condition for both, structures with and without coatings, as it is necessary to have better statistics of fabricated lasers reliability.

## Acknowledgements

This work has been supported by the State Committee for Scientific Research (KBN) grant PBZ-023-10.

 

## References


1. T. Strite and G. Hoven, "Trends in pump laser diode markets and technology", *Lightwave*, Feb. 1999, 55–62 (1999).
2. J.J. Coleman, "Strained-layer quantum well heterostructure lasers," *Thin Solid Films* **216**, 68–71 (1992).
3. S.D. Offsey, W.J. Schaff, L.F. Lester, L.F. Eastman, and S.K. McKernan, "Strained-layer InGaAs-GaAs-AlGaAs lasers grown by molecular beam epitaxy for high speed modulation," *IEEE J. Quan. Elect.* QE **27**, 1455–1462 (1991).
4. M. Bugajski, M. Kaniewska, K. Regiński, A. Maląg, S. Łepkowski, and J. Muszalski, "GRIN SCH SQW AlGaAs/GaAs lasers grown by molecular beam epitaxy: Modelling and operating characteristics," *Proc. SPIE* **3186**, 310 (1997).
5. M. Bugajski, M. Kaniewska, K. Regiński, J. Muszalski, D. Kryńska, and A. Litkowiec, "GRIN SCH SQW AlGaAs/GaAs lasers grown by molecular beam epitaxy," *Electron Techn.* **29**, 346–350 (1996).
6. PICS 3D Instruction Manual, Crosslight Software Inc., CA 1998.
7. S.L. Chuang, "Efficient band-structure calculation of strained quantum-wells," *Phys. Rev.* B **43**, 9649–9661 (1991).
8. W.W. Chow, S.W. Koch, and M. Sargent III, *Semiconductor Laser Physics*, Springer-Verlag, Berlin Heidelberg, 1994.
9. K. Regiński and M. Bugajski, "MBE technology of semiconductor quantum well lasers," *Optoelectr. Rev.* **4**, 101–116 (1996).
10. J. Kątcki, J. Ratajczak, J. Adamczewska, F. Phillip, N.Y. Jin-Phillip, K. Regiński, and M. Bugajski, "Formation of dislocations in InGaAs/GaAs heterostructures," *Physica Status Solidi (a)* **171**, 275–282 (1999).
11. J. Kątcki, J. Ratajczak, F. Phillip, N.Y. Jin-Phillip, M. Shiojiri, K. Regiński, and M. Bugajski, "TEM study of the formation of defects in AlGaAs/GaAs and InGaAs/GaAs heterostructures," *Electr. Techn.* **32**, 343–347 (1999).
12. S.L. Chuang, *Physics of Optoelectronic Devices*, Wiley Interscience Publication, New York, 1995.
13. M. Bugajski and M.Godlewski, "Optical probing of interface disorder in semiconductor nanostructures," *Electr. Techn.* **31**, 159–161 (1998).
14. M. Bugajski, *Low Dimensional Semiconductor Structures*, TEMPUS Series in Applied Physics, Warsaw University of Technology, Warsaw 1997.
15. M. Bugajski, P. Edelman, M. Wesołowski, J. Ornoch, W. Lewandowski, and K. Kucharski, "Non-destructive, whole wafer imaging of semiconductors by photoluminescence scanning", *Materials science and engineering B, Solid State Materials for Advanced Technology*, B **20**, 186–189 (1993).
16. M. Bugajski, B. Mroziewicz, K. Regiński, M. Zbroszczyk, and A. Maląg, "InGaAs/GaAs optical laser pumps for fibre amplifiers of EDFA type," *Proc. VI Symp. Laser Technology*, Szczecin-Świnoujście, 137–141 (1999). (in Polish)
17. M. Bugajski, K. Regiński, B. Mroziewicz, J.M. Kubica, P. Sajewicz, T. Piwoński, and M. Zbroszczyk, "High-performance 980-nm strained-layer InGaAs/GaAs quantum-well lasers", *Opt. Appl.*, (2001). (to be published)
18. T. Piwoński, P. Sajewicz, J.M. Kubica, M. Zbroszczyk, K. Regiński, B. Mroziewicz, M. Bugajski, "Long-wavelength strained-layer InGaAs/GaAs quantum-well lasers grown by molecular beam epitaxy", *Microwave and Optical technology Letters*, (2001). (to be published)
19. P. Sajewicz, T. Piwoński, K. Regiński, B. Mroziewicz, and M. Bugajski, "Highly reliable CW strained layer InGaAs/GaAs ($\lambda$ = 980 nm) SCH SQW lasers fabricated by MBE", *Proc. 3rd Int. Conf. Advanced Semiconductor Devices and Microsystems, ASDAM 2000*, Smolenice, Slovakia, 411–414 (2000).
20. A. Larsson, J. Cody, and R.J. Lang, "Strained-layer InGaAs/GaAs/AlGaAs single quantum well lasers with high internal quantum efficiency, *Appl. Phys. Lett.* **55**, 2268–2270 (1989).
21. A. Larsson, S. Forouhar, J. Cody, R.J. Lang, and P.A. Anderson, "A 980 nm pseudomorfic single quantum well laser for pumping erbium-doped optical fibre amplifiers," *IEEE Photonic Technology Letters* **2**, 540–542 (1990).
22. C. Shieh, J. Mantz, H. Lee, D. Ackley, and R. Engelman, "Anomalous dependence of threshold current on stripe width in gain-guided strained-layer InGaAs/GaAs quantum well lasers," *Appl. Phys. Lett.* **54**, 2521–2523 (1989).
23. K.J. Beernink, P.K. York, and J.J. Coleman, "Dependence of threshold current density on quantum well composition for strained-layer InGaAs-GaAs lasers by metalorganic chemical vapor deposition," *Appl. Phys. Lett.* **55**, 2585–2587 (1989).
24. K.J. Beernink, P.K. York, J.J. Coleman, R.G. Waters, J. Kim, C.M. Wayman, "Characterisation of strained-layer InGaAs-GaAs lasers with quantum wells near the critical thickness," *Appl. Phys. Lett.* **55**, 2167–2169 (1989).
25. H. Horie, H. Ohta, and T. Fujimori, "Reliability improvement in 980-nm laser diodes with a new facet passivation process", *IEEE J. Selected Topics in Quantum Electronics* **5**, 832–838 (1999).
26. M. Okayasu, M. Fukuda, T. Takeshita, and S. Uehara, "Stable operation (over 5000 h) of high power 0.98 μm InGaAs-GaAs strained quantum well ridge waveguide lasers for pumping $Er^{3+}$-doped fibre amplifiers," *IEEE Photonic Techn. Lett.* **PTL-2**, 689–691 (1990).
27. M. Fukuda, M. Okayasu, J. Temmyo, and J. Nakano, "Degradation behaviour of 0.98-μm strained quantum well InGaAs/AlGaAs lasers under high-power operation," *IEEE J. Quantum Electronics*, QE **30**, 471–476 (1994).
28. S.E. Fischer, R.G. Waters, D. Fekete, J.M. Ballantyne, Y.C. Chen, and B.A. Soltz, "Long-lived InGaAs quantum well lasers," *Appl. Phys. Lett.* **54**, 1861–1863 (1989).